Journal of Materials Chemistry A

Accepted Manuscript

ROYAL SOCIETY OF CHEMISTRY

www.rsc.org/materialsA

Journal of Materials Chemistry A RSCPublishing

ARTICLE

Failure analysis in ITO-free all-solution processed organic solar cells

Cite this: DOI: 10.1039/xoxxoooooox

Received ooth January 2012,
Accepted ooth January 2012

DOI: 10.1039/xoxxoooooox

www.rsc.org/

Y. Galagan,[*a] T.M. Eggenhuisen,[b] M.J.J. Coenen,[b] A.F.K.V. Biezemans,[c] W.J.H. Verhees,[c] S.C. Veenstra,[c] W. A. Groen,[b,d] R. Andriessen[a], R. A. J. Janssen[e]

In this paper we discuss a problem-solving methodology and present guidance for troubleshooting defects in ITO-free all-solution processed organic solar cells with an inverted cell architecture. A systematic approach for identifying the main causes of failures in devices is presented. Comprehensive analysis of the identified failure mechanisms allowed to propose practical solutions for further avoiding and eliminating failures in all-solution processed organic solar cells. Implementation of the proposed solutions has significantly improved the yield and quality of all-solution processed organic solar cells.

Introduction

During the last decade organic photovoltaics (OPVs) attracted a lot of attention due to its high potential for roll-to-roll solution processing [1-5]. Deposition of all layers by printing and coating guarantees low manufacturing cost [6-8], thereby making OPV competitive with conventional silicon photovoltaics. All-solution processed OPV cells and modules have been successfully demonstrated more than once by different groups [9-14]. The next step towards industrial manufacturing and up-scaling of these approaches is roll-to-roll processing, which requires high manufacturing yield. Sequential deposition of six [14], or more, defect-free solution processed layers with thicknesses in the range of 30-200 nm can be very challenging even for lab scale devices. Increasing the active area of the cells and modules generally reduces the production yield due to an increasing amount of defects. The first step to reduce or completely eliminate these defects is the identification of such defects and the causes that have led to their appearance. Thus, a comprehensive functional analysis is required as an input to determine the relevant failure modes. Correct understanding of the failure mechanisms can provide effective guidance on how to significantly reduce or completely eliminate the considered failure in the OPV cells and modules.

The reason to start this study was the observed low manufacturing yield for all-solution OPV devices with following six printed/coated layers: Ag-grid/PEDOT:PSS/ZnO/P3HT:PCBM/PEDOT:PSS/Ag [14]. Most of these devices required the application of short electric pulses at relatively high voltage to start working properly. Such electric pulses may seem to be an integral part of the manufacturing process, but a certain percentage of the devices worked decently without applying any high voltage treatment. This observation triggered us to set-up a structured investigational approach for understanding and identifying the failure mechanisms observed in the devices with the proposed stack. A major requirement for successful and sustainable solutions for the observed problems by troubleshooting procedures is to gather all necessary information related to the problem envisaged, including all details of the occurring processing (sub-)steps. As there are many separate sources of information, all available and detailed information has to be gathered, integrated and analysed to understand the cause of the failure envisaged in the devices. If successful, this analysis will help to eliminate the failure in all further devices by implementing the required remedying procedures.

Although in this study the systematic approach for identifying the failure mechanism is presented for only one OPV device stack, the proposed problem solving methodology

a - Holst Centre - Solliance, High Tech Campus 21, 5656AE, Eindhoven, the Netherlands; E-mail: yulia.galagan@tno.nl (Y. Galagan)
b - Holst Centre/TNO, High Tech Campus 31, 5656AE, Eindhoven, the Netherlands;
c - Energy Research Centre of the Netherlands (ECN) - Solliance, High Tech Campus 21, 5656AE Eindhoven, the Netherlands
d - Faculty of Aerospace Engineering, Delft University, Kluyverweg 1, 2629 HS Delft, The Netherlands
e - Eindhoven University of Technology – Solliance, Postbus 513, 5600 MB Eindhoven, the Netherlands

can be adapted for other types of devices. The major benefits from understanding the failure mechanism are the following: early identification and elimination of potential failures, problem prevention, reduced time for the development of new and better performing device stacks and reduced associated cost, improved quality and reliability of manufactured OPV devices, significantly improved production yield, and thereby ultimately reduced manufacturing cost. Current work can be considered as a guidance for troubleshooting defects in the solution processed organic electronic devices.

Experimental

All-solution processed OPV devices investigated in this study were produced on 3x3 cm^2 glass substrates and have the layer sequence as shown in Figure 1a:

glass/Ag-grid/PEDOT:PSS/ZnO/P3HT:PCBM/PEDOT:PSS/Ag

All layers in the devices were inkjet printed, unless otherwise stated and all device fabrication steps were performed under "clean-room 1000" conditions.

Ag grids and busbars (both front and back) were inkjet printed using a Fujifilm Dimatix Materials Printer (DMP 2831). Sintering was performed in air or in N_2 for the front and back electrode, respectively. Inkjet printing of high conductive poly(3,4-ethylenedioxythiophene) : poly(styrenesulfonate) (HC PEDOT:PSS), ZnO nanoparticles (ZnO NP), the photo-active layer (PAL) and second PEDOT:PSS was performed on a LP50 printing platform (Pixdro, Roth&Rau) using an industrial printhead (KM512LN, 3.5 cm width, 360 DPI nozzle spacing) and non-halogenated solvents only. ZnO nanoparticles were synthesized according to literature procedure [34] using the hydrothermal condensation of Zn(acetate). After several rinsing steps, the nanoparticles were re-dispersed in a veratrole:*o*-xylene mixture with a concentration of 17.5 mg/ml. For the photo-active layer an ink consisting of o-xylene, indane and tetraline (1:1:1) was used with a 1.3 wt% concentration of both

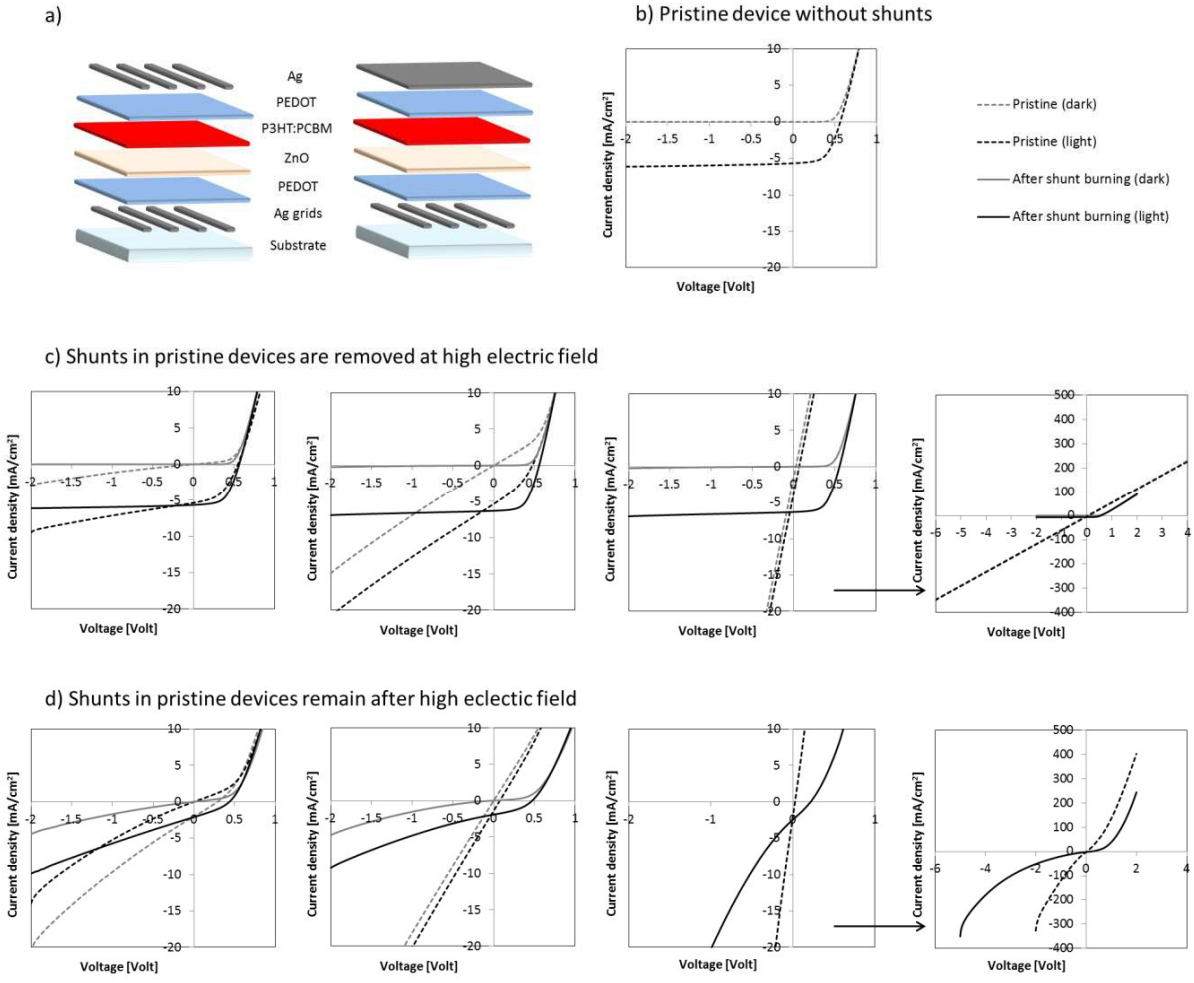

Fig. 1 A schematic illustration of the typical all-solution processed OPV device (a); Typical JV curves of the OPV devices before and after post-treatment with short electric pulse: (b) – a device that does not require a post-treatment, (c) – devices with different types of shunts which disappear after post-treatment, (d) – devices with shunts that cannot be removed with post -treatment.

P3HT and PCBM, yielding a layer with ~240 nm thickness. On top of the inkjet printed photo-active layer a 200 nm thick PEDOT:PSS layer (Orgacon S315) was printed. The manufacturing process for the devices is described in details elsewhere [14, 16]. For a better understanding of possible issues with the back electrode, sometimes in selected devices an evaporated MoO_3/Ag back electrode was used instead of the printed PEDOT:PSS/Ag back electrode.

Solvents were acquired from Sigma-Aldrich and used as received. HC PEDOT:PSS (Agfa, Orgacon-IJ 1005) was mixed with 15 wt% 2-butanol resulting in a drop in surface tension from 35.6 $mN \cdot m^{-1}$ to 24.0 $mN \cdot m^{-1}$. PEDOT:PSS (Agfa, Orgacon S315), Poly-(3-hexylthiophene) (P3HT, Merck, Lisicon SP001, Mw ~19 kg/mol,), and [6,6] phenyl C61-butyric acid methyl ester (PCBM, 99%, Solenne BV), Suntronic U5603 Ag nanoparticle ink (Sun chemicals, Slough, UK) were used as received.

Layer thicknesses were obtained by Dektak profilometry (Veeco). Cross sections for analysis with scanning and transmission electron microscopy (SEM and TEM) were prepared using a Nova 200 Nanolab Small Dual Beam. Before preparation, a thin Pt layer is deposited on the entire sample in a sputter coater to avoid charging. Subsequently, a 500 nm Pt layer is deposited using electron beam induced deposition and a 1.5 µm Pt layer is deposited using ion beam induced deposition on the region of interest to protect the sample during preparation. As a final cleaning step, a 5 kV milling step was performed. TEM studies were performed using a TECNAI F30ST TEM operated at 300kV. Non-contact atomic force microscopy (NC-AFM) measurements were performed on a NX-10 AFM (Park Systems) using a PPP-NCHR non-contact cantilever (Park Systems), having a nominal resonance frequency of 330 kHz and a force constant of 42 N/m. Current–voltage (J-V) curves were measured using simulated solar light in a home built set-up with a halogen lamp (100 mW/cm^2) calibrated with a Si reference cell and using a shadow mask for 1 cm^2 devices.

Results and discussion

The "baseline" process for all-solution processed OPV devices presented and described in [14] is a result of the comprehensive analysis described in this publication. It allows to largely eliminate most of the failures observed in the "first generation" of all-solution processed OPV devices, where only a certain (low) percentage of the OPV devices shows the desired photovoltaic behaviour (Fig. 1b). All other devices show large deviations from this "ideal" or normal JV curve. Substantial current leakage or even a complete short circuit can be readily observed (Fig. 1c-d). Applying a high voltage (typically -10V) restores in most cases the JV-curve to normal, as shown in Fig. 1. The treatment of OPV devices with a short electrical pulse with a high current density, as a post-treatment step have been described by Larsen-Olsen *et al.* [17] These authors propose that the post treatment step is required to convert the pristine and non-functional multilayer-coated stack into a functional solar cell through the formation of a charge selective interface. After the fast post-treatment step the device stack becomes active and all devices are functional. Besides this, it is well known that short electric pulses with high current density can burn out shunts in the device, if such are present. In our case the characteristics of the JVs of pristine devices were quite variable, and a short electrical post-treatment often helped to get functional devices (Fig. 1c). However, occasionally such electrical pulse did not have any positive effect and the current leakage remained more or less the same for these devices, as shown in Fig. 1d. This indicates that there is probably more than one failure mechanism present in the devices. The comprehensive analysis identified to the following possible failures (or combinations thereof) in the devices:

- *Short circuit due to direct contact of bottom current collecting grids and top electrode* caused by the specific topology of the grids. Current collecting grids used as a bottom electrode in OPV devices are in this case [14] made by inkjet printing of Ag nanoparticles inks. The average height of the grids is in the range of 300 nm and the average width is between 150-300 µm. With such very high ratio between width and height, the current collecting grids can be considered as very flat objects spread in lateral direction. However, due to imperfections of the printing, drying and sintering processes, local spikes and non-uniformities are formed on the grids. These local imperfections can propagate in the subsequent layers, which can ultimately lead to direct contact of the bottom grid and top electrode, as shown in Figure 2 (b).

- *Short circuit due to direct contact of two PEDOT:PSS layers*: This case is very often observed in devices with spin coated layers. Two highly conducting PEDOT:PSS layers can

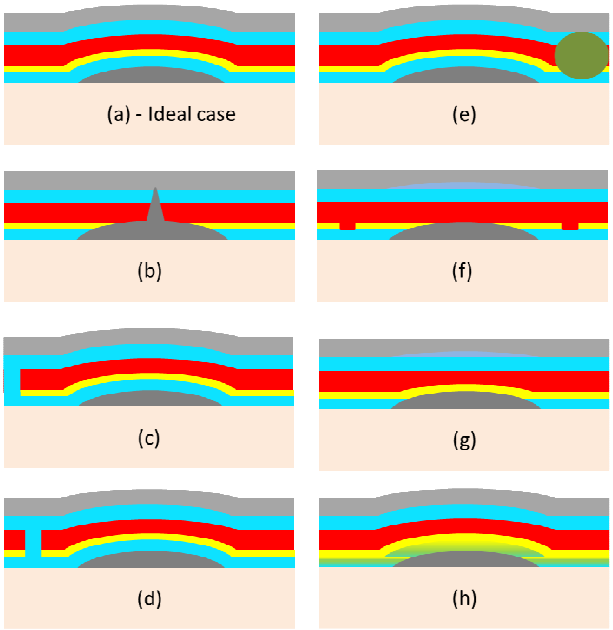

Fig.2. Schematic illustration of the OPV devices stack with different failure mechanisms: (a) – ideal case; (b) – direct contact of bottom Ag grid and top PEDOT:PSS/Ag; (c) – contact between top and bottom PEDOT:PSS layers at the edge of the device; (d) – pinholes in photoactive layer leading to contact between top PEDOT:PSS and bottom ZnO/PEDOT:PSS; (e) – particles in one of the layers; (f) – pinholes in ZnO layer; (g) - absence of bottom PEDOT:PSS layer; (h) – interaction between bottom PEDOT:PSS and ZnO.

easily be contacted at the edge of the substrate (Figure 2 (c)). Use of printing methods often solves this problem, because the top and bottom PEDOT:PSS layers can be patterned in such way to avoid direct contact at the edges of the device.

- *Short circuit or shunts due to direct contact of bottom and top electrode* due to pinholes and defects in the photoactive layer. The photoactive layer is the fourth layer in the device stack. All defects in underlying layers promote defects formation and non-uniformities in the photoactive layer. Due to non-uniformities in the photoactive layer a direct contact between top and bottom electrode can occur (Figure 2 (d)).

- *Short circuit due to particles*: Two types of particles should be considered: isolating particles (non-conductive) and conductive particles. The latter can cause a local shunt due to its conductive properties. This is expected to be the most common cause of short circuit in organic electronic devices. Wherein, the amount and size of the particle can be very diverse. The origin of the particles is also different, ranging from dust particles to non-dissolved or aggregated particles of the actual functional material (Figure 2 (e)). Moreover, wetting on top of the particles (either conductive or not) will create two possibilities: good wetting or de-wetting. With good wetting, the particle will be covered with subsequent layer and it should not have big influence on the devices performance. If the wetting is not good, in most cases one or other subsequent layers will not be present on top of the particle and in most cases around the particle. The latter can be considered as a "circular pinhole" (local de-wetting around the particle).

- *Pinholes and defects in the ZnO layer*: Defects and pinholes in ZnO layer will result in local variations in work function at the interface with photoactive layer. These non-uniformities in the interfacial layer become efficient points for a current leakage and charge recombination. The local absence of ZnO will remove the electrical asymmetry in the devices, as in that case the photoactive layer will be on both sides into contact with PEDOT:PSS layers. This case is schematically depicted in Figure 2 (f). It shows that a perfectly closed ZnO layer is a necessity for proper working pristine devices.

- *Pinholes and defects in the bottom PEDOT:PSS layer*: Theoretically this case should not provoke big problems. Depending on its relative and absolute area contribution, (local) absence of the bottom PEDOT:PSS layer can possibly cause problems with the lateral conductivity. This in turn can increase the series resistance of the device. In case of closeness of the subsequent layer(s) such devices still will function, with only a slightly decreased J_{sc}, due to reduced active area of the electrode. However, to get a closed ZnO layer on top of a defects-rich PEDOT:PSS layer is almost impossible. Defects in PEDOT:PSS layer will cause also defects in the ZnO layer, which will lead to additional issues as described in previous paragraph.

- *Interaction between PEDOT:PSS and ZnO:* A combination of PEDOT:PSS-ZnO has been used more than once in all-solution processed single junction organic solar cells [3, 14, 16-18] as well as a recombination layer in tandem devices [19]. The electrons collected by ZnO should be effectively transported to the corresponding contact being a through p-type PEDOT:PSS layer. Proper functioning of the solar cells is only possible if PEDOT:PSS and ZnO form equivalent ohmic contacts. However, as has been shown [19], not all combinations of PEDOT:PSS and ZnO are equally good. In addition, an often observed drop in conductivity of the PEDOT:PSS layer, after deposition of ZnO, points on a strong ((electro-)chemical) interaction between these two layer (see below).

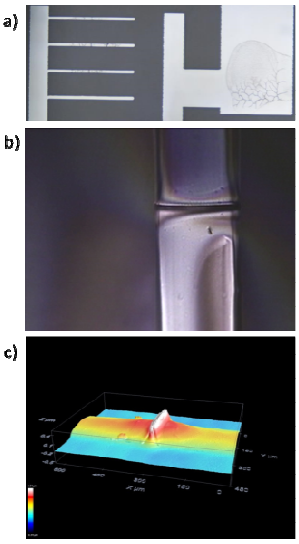

Fig. 3. Optical microscope (a, b) and confocal microscope (c) images showing the cracks in inkjet printed Ag structures after deposition of PEDOT:PSS.

- *Redox behaviour of PEDOT:PSS.* The presence of two PEDOT:PSS layers in one single device stack and its effect on the functioning of the device is still a subject to discussions. It was found and confirmed in other publications [17] that devices with two PEDOT:PSS layers require a short electric pulse to start functioning. We found that redox properties of PEDOT:PSS are responsible for this phenomenon. A detailed analysis of this and all other possible causes leading to a failure in the devices is discussed below.

Substrates

The substrates for OPV devices must satisfy numerous requirements, such as:

- Optical quality and transparency, *i.e.* that a large fraction of the incident sunlight can reach the photoactive layer;

- Substrate smoothness in the nanometre range to provide a surface that will promote high-quality deposition of subsequent layers. Substrates should be free from spikes, because spikes or irregularities of substrates can penetrate into the device layers which in turn can lead to unwanted local short circuits;

- The ability to support processing at sufficiently high temperatures;

- Good dimensional stability;

- Good resistance to the chemicals used during processing;

- Low water absorption.

The right choice of substrate is a first step towards successful deposition of all subsequent layers. In these study we

use glass substrates. Glass fits most of the requirements, although it has some limitation for roll-to-roll processing. Nevertheless, the goal of this study is to have a close look into the devices stack and identify the main causes leading to the failures in the devices.

Thus, the main two requirements for the glass substrate are its surface quality and surface energy. The surface quality of the substrates for OPV applications is mainly determined by surface roughness (smoothness) and surface cleanliness [20]. Surface smoothness is largely defined by the internal cleanliness of the film substrate and typified by the absence of peaks with sizes ranging from tens to hundreds of nanometers. In this study display quality Eagle 2000 glass substrates were used, which guarantee very high smoothness of the surface. Surface cleanliness is determined by the presence of dust and surface scratches. These defects can range in size up to tens of micrometers both laterally and vertically, and are unavoidable in substrates that are handled in a non-clean room environment. Therefore, proper cleaning of the substrates is an essential process prior to the processing of the subsequent electro-active layers. Most of the potential deteriorating dust particles can be removed by surface cleaning.

A proper and homogeneous surface energy of the substrate[21] is another critically important parameter for successful deposition of the subsequent layers from solution. The surface energy is a direct manifestation of intermolecular tension. Molecules at the surface are not surrounded by other molecules, so the molecular forces are unbalanced and the molecules have additional energy compared to the molecules inside the bulk of the liquid or solid. The surface or interfacial tension is expressed in $J \cdot m^{-2}$ ($N \cdot m^{-1}$) or in $erg \cdot cm^{-2}$ ($dyn \cdot cm^{-1}$). The surface energy of the substrates can be modified by flame treatment, corona discharge treatment, ozone or plasma treatments, all of which impart some oxidation to the surface and promote adhesion for printing of subsequent layers.

Front Ag grids

The first printed layer in the all-solution processed OPV stack is the Ag grid. There are two important parameters determining the quality of printed grids: the adhesion of the Ag grid to the substrate and completeness of sintering. Adhesion of the inkjet printed Ag grid very much depends on the surface energy of the substrate. The completeness of the sintering will determine the final resistance of the grids and a successful removal of the voids between the Ag nanoparticles. The most common approach to achieve high conductivities in printed silver nanoparticle structures is by thermal [22], laser [23], microwave [24] or photonic flash sintering [15]. During the sintering process, the polymer shell that stabilizes the ink by preventing the silver nanoparticles from agglomerating, is partially removed. Subsequently, the nanoparticles fuse and form a continuous network of conductive pathways. During this process, the removal of voids between the Ag particles and especially between the particles and substrate, is extremely important. Incomplete sintering will allow penetration of the subsequent PEDOT:PSS ink into the voids of the Ag structures. This in turn can lead to wrinkling and cracking of Ag structures. As a result, Ag structures lose their integrity, and spikes with high topology are formed, as shown in Figure 3.

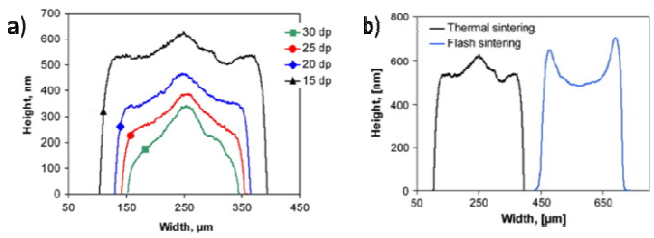

Fig. 4. Typical cross sectional profiles of inkjet printed Ag grid lines: (a) – printed with different dot pitches (reproduced from [9] with permission, Copyright 2012, Elsevier B.V.), (b) – with thermal and flash sintering (reproduced from [15] with permission, Copyright 2012, Elsevier B.V.).

The cross sectional profile of inkjet printed grid lines, as shown in Fig. 4, depends on many issues, such us: printing parameters; merging ability of the individual droplets, which is determined by the surface energy of the substrate and surface tension of the ink; solid content of the ink; ink composition and presence of surfactants; drying and sintering conditions, etc. For example, Chen et al. [25] have shown that the cross-sectional profile of silver nanoparticle inks with water-based solvents by inkjet printing very much depends on the drying condition and humidity, resulting either in concave profiles or convex profiles. Galagan et al. [9, 15] have shown that the cross section of inkjet printed silver structures depends on dot pitch and strongly on the sintering method, which leads to different widths and topologies of the grid lines (Fig. 4b).

Front PEDOT:PSS

Deposition of PEDOT:PSS proved to be the most challenging step in this device architecture, because it has to be deposited on a heterogeneous surface comprising both the bare glass substrate and the printed Ag. The feasibility of proper layer deposition (in our case inkjet printing of PEDOT:PSS) on heterogeneous surfaces, very much depends on the contact angles of PEDOT:PSS on these dual surfaces. When the contact angle of the PEDOT:PSS ink on one surface is substantially smaller than on the other, the droplet would shift in the direction of higher surface energy. The large difference in contact angle and surface energy gradient can lead to a concentration gradient: surface tension will naturally cause the liquid to flow away from the regions of low surface energy. The glass substrate typically has a much higher surface energy than the printed Ag grid. Hence, by following the principle described above, a wet PEDOT:PSS layer will move into the direction away from the regions with low surface energy. As a result, de-wetting of the Ag grid can occur and a cross sectional profile of PEDOT:PSS layer between the two Ag grid line has a thickness gradient, as shown in Figure 5 (a). Surface treatments can increase the surface energy of the Ag grid, which most likely will improve wettability of the PEDOT:PSS. However, it is important to note two important issues: (1) atmospheric

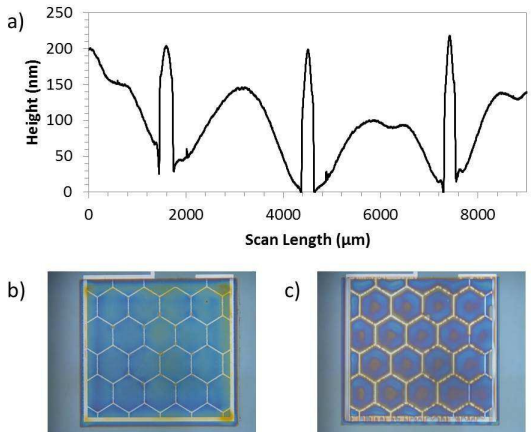

Fig. 5. (a) – Dektak profile of the glass substrate contained inkjet printed Ag grids and PEDOT:PSS layer; (b) – optical microscope image of a surfactant modified inkjet printed PEDOT:PSS on the plasma-treated heterogeneous glass/Ag-grid substrate; (c) inkjet printed non-modified PEDOT:PSS on non-treated glass/Ag-grid substrate, resulting in de-wetting of the grid and in a gradient of PEDOT:PSS thickness.

plasma treatments can lead to oxidation of metal tracks and (2) by treatment of metal structures the substrate is also affected and increases its surface energy, hence it can lead to the same issues of printing on heterogeneous surface.

Another solution is to add a surfactant to the PEDOT:PSS solution. In aqueous coatings, surfactants are almost always used at relatively high concentrations above the critical micelle concentration [26]. As a consequence, the surface is saturated with surfactant molecules. The surface tension then remains constant and rarely is the cause of any defects. Figure 5 (b) shows an optical microscope image of surfactant modified inkjet printed PEDOT:PSS on a plasma-treated heterogeneous glass/Ag-grid substrate, while Figure 5 (c) shows inkjet printed non-modified PEDOT:PSS on non-treated glass/Ag-grid surface, resulting in de-wetting of the grid and in a gradient in the PEDOT:PSS thickness.

Besides the defects related to difference in surface energy, incomplete coverage of Ag grids may also appear if the topology or the grid is too high. We previously reported [9] the influence of grid topology on device performance. Although, increasing grid topology improves grid conductivity and improves the fill factor, above a certain grid height it was not possible to produce short circuit free devices. Thus, control of the grid topology is a very important parameters towards successful manufacturing of the devices.

High topology of the grid and bad grid coverage by PEDOT:PSS very often appears to be a main reason for bad functionality of the devices as it leads in most cases to short circuits. Fig. 6b depicts a thermography image of the non-functional device (for the reference, the device layout is depicted in Fig. 6a). As can be observed from the image, the heat generation is represented as random points located at the current collecting grids lines. Most likely the current collecting grid has a higher topology at these points and are not planarized by the subsequently deposited layers PEDOT:PSS/ZnO/photoactive layer. Applying a high voltage (-10 V) leads to burning out of the defects, resulting in properly functioning devices. The thermography images of the devices after "shunt burning" are shown in Fig. 6c. The JV curves of the device before and after "shunt burning" are shown in Fig. 6d. Optimization of grids topology, wetting of PEDOT:PSS on Ag grids and substrate, and optimization of printing the subsequent layers (ZnO, PAL) can provide functional devices without "shunt burning".

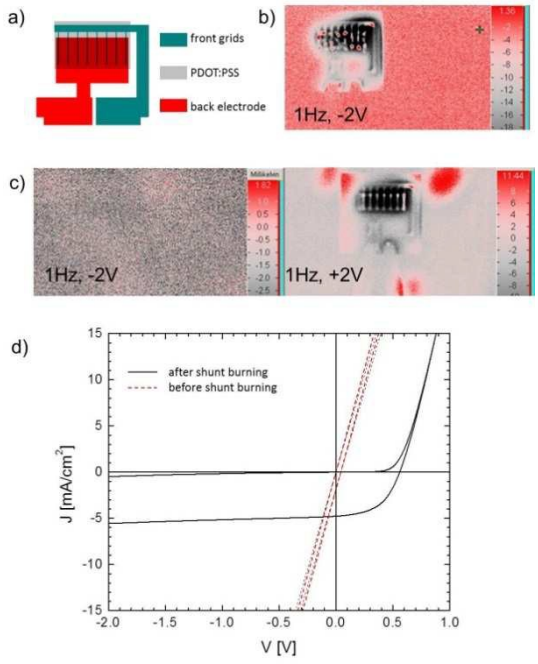

Fig. 6. (a) – Device layout depicted the overlap of two electrodes (front current collecting grids with PEDOT:PSS/ZnO and back Ag electrode); (b) - thermography image of the non-functional device at -2V; (c) - thermography images of the device after "shunts burning" at -2V and +2V; and correspondent JVs of the device before and after "shunts burning".

ZnO layer

As an n-type inorganic semiconductor, ZnO has been widely used in organic solar cells. Its application in all-solution processed devices is supported by low cost, easy synthesis, non-toxicity, high stability, low temperature curing and the ability to be solution processed. ZnO serves as an electron transport layer in single junction OPV devices and the

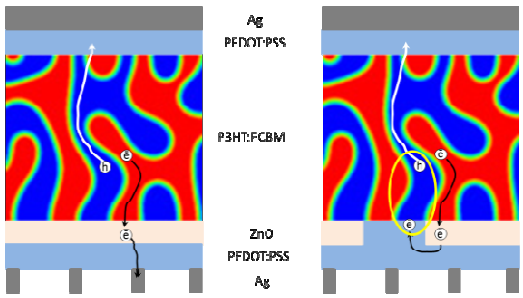

Fig. 7. Schematic illustration of the OPV devices showing the charges flow.

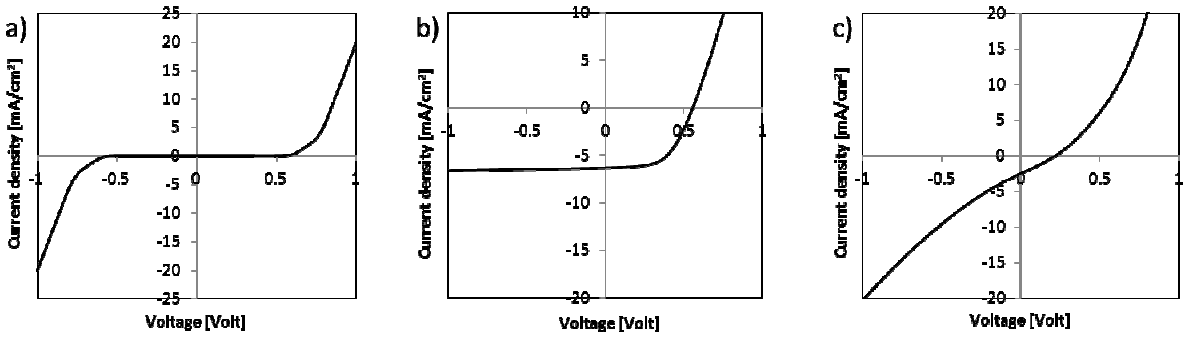

Fig. 8. Typical JVs of illuminated device with (a) - symmetric electrodes, (b) – standard diode behaviour in OPV cells and (c) – result of parallel connection of several symmetric and normal devices.

combination of PEDOT:PSS/ZnO is acting as a recombination layer in tandem devices [19]. Moreover, the combination of PEDOT:PSS/ZnO more than once has been used in all-solution processed single junction solar cells [11, 12, 14, 16, 18], where the ZnO layer is responsible for the electron transport, and the PEDOT:PSS provides lateral conductivity. With this, the electrons collected by ZnO should be effectively transported through the p-type PEDOT:PSS layer. A good functioning of devices is possible only if PEDOT:PSS and ZnO form ohmic contacts.

One of the challenges in the processing of OPV devices is to make a complete pinhole- and defect-free ZnO layer on top of the PEDOT:PSS layer. Defects and pinholes in the ZnO layer will result in local variations in work function at the interface with photoactive layer. Thus, such non-uniformities in the interfacial layer become efficient points for current leakage and charge recombination, as shown in Fig. 7.

The local absence of the ZnO layer creates a symmetric device where the photoactive layer is sandwiched between two PEDOT:PSS layers. The typical IV curve of symmetric devices is shown in Fig. 8a. However, in real devices, defects in ZnO layer creates only some islands with symmetric electrodes, the rest of devices has different, asymmetric, electrodes (Fig 8b). The total active area of the device can be represented as a parallel connection of several symmetric and normal devices. The Final JV of such device depends on the ratio between symmetric and normal areas, a typical example is shown in Fig. 8c.

The continuity of the ZnO layer depends largely on the quality of PEDOT:PSS layer. A defect-free PEDOT:PSS layer provides an uniform surface for a subsequent deposition of the ZnO layer. However, the presence of defects and holes in the PEDOT:PSS layer leads to deposition of ZnO layer on surfaces with different surface energies, either PEDOT:PSS, Ag grids, substrate or particles. Furthermore, the ZnO layer is the thinnest layer in the device stack, with a typical thickness of approximately 30 nm, making it the most difficult one for creating a closed layer. In addition, the ZnO solution has a low viscosity. Hence, proper and closed deposition of a very thin layer from a low viscous solution on a heterogeneous surface is a big challenge for inkjet printing.

The formation of a ZnO layer was investigated on homogeneous and heterogeneous surfaces. A surface for deposition of the ZnO layer consisted of glass with inkjet

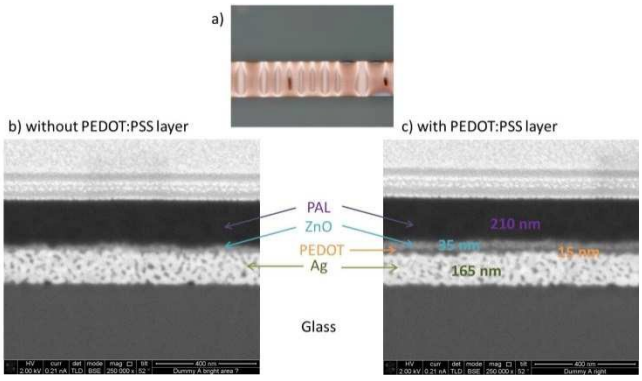

Fig. 9. (a) – optical microscope image of inkjet printed Ag line with unmerged droplets of inkjet printed PEDOT:PSS (Reproduced from Ref. [14] with permission from The Royal Society of Chemistry); SEM micrographs of FIB cross sections of the Ag line: (b) without PEDOT:PSS and (c) with PEDOT:PSS.

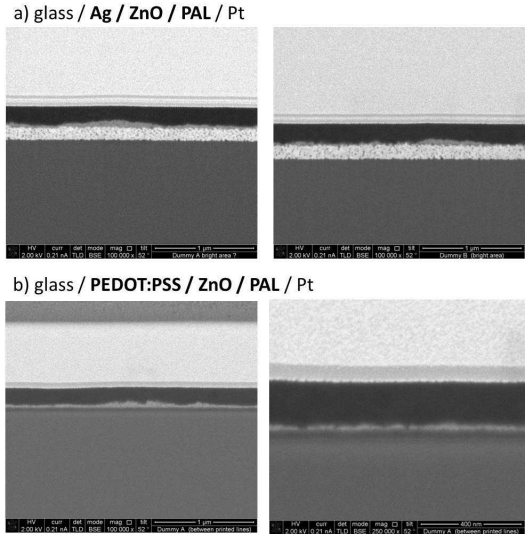

Fig. 10. SEM micrographs of FIB cross sections of (a) – glass/Ag/ZnO/Photoactive layer/Pt, (b) - glass/PEDOT:PSS/ZnO/Photoactive layer/Pt.

printed current collecting grids covered with PEDOT:PSS. To obtain a heterogeneous surface we used a sample where PEDOT:PSS layer contained a lot of pinholes and inhomogeneities. Fig. 9a shows a single Ag line and a PEDOT:PSS layer with a droplet pattern because the inkjet printed droplets have not merged properly. This results in a PEDOT:PSS layer with pinholes. Subsequently, the quality of the printed ZnO layer on such a heterogeneous surface is investigated. A cross-section image was made by using focused ion beam milling (FIB) at the area with and without PEDOT:PSS layer (Fig. 9a). The corresponding SEM images (Fig. 9b-c) display the presence of a ZnO layer at both regions with and without the PEDOT:PSS layer.

A more detailed analysis reveals ZnO layer thickness inhomogeneities, mostly in the areas without a PEDOT:PSS layer (Fig. 10a). However, similar ZnO layer inhomogeneities were also observed on top of very uniform glass/PEDOT:PSS surfaces (Fig. 10b). In addition, a spin coated ZnO layers typically have less issues with layer uniformity compared to an inkjet printed layers. The issue of ZnO layer uniformity in inkjet printed devices can be rather simply solved by the subsequent printing of two ZnO layers. Subsequent printing not only increases the thickness of the ZnO layer if the ink nor inkjet print setting remains unchanged. It also seems to flatten existing inhomogeneities in the first printed layer [16]. Thus, increasing of the ZnO layer thickness significantly increases the yield of the devices.

To conclude, if holes and non-uniformities in the ZnO layer are still present in the device, it creates effective areas for current leakage due to charge recombination. This type of current league cannot be removed by post-treatment with a short electric pulse. The typical J-Vs corresponding to this situation are shown in Fig. 1d.

PEDOT:PSS and ZnO interaction

The combination of PEDOT:PSS and ZnO remains to be a subject for further investigation. As has been shown [19], not all combinations of PEDOT:PSS and ZnO are compatible in a device stack. Thus, introducing a PEDOT:PSS layer between ITO and ZnO in typical single junction devices with an inverted architecture exhibits different behaviour depending on the type of PEDOT:PSS formulation used. Inserting an extra p-type buffer layer between ITO and ZnO normally introduces a barrier, because the electrons collected by the ZnO layer are not able to reach the ITO electrode [19]. For efficient charge transport an ohmic contact between PEDOT:PSS and ZnO is required.

In addition to losses due to this barrier, the conductivity of PEDOT:PSS is different before and after deposition of ZnO. A decreased conductivity of the PEDOT:PSS layer after deposition of the ZnO layer indicates an interaction between these two layer. High conductivity is a necessary property of PEDOT:PSS used in all-solution processed devices, as it is required for the lateral conductivity between the grid lines. The resistance of the PEDOT:PSS layer was determined by four probes measurements with evaporated Ag contacts and the

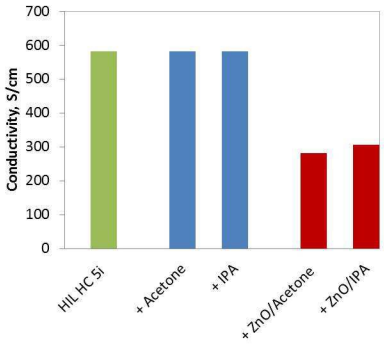

Fig. 11. Conductivity of PEDOT:PSS (HC HIL5i) spin coated on glass, and after spin coating pure solvents (acetone and isopropanol) and ZnO nanoparticles in acetone and isopropanol.

conductivity was calculated taking into account the geometry of the evaporated contacts and thickness of the PEDOT:PSS layer. Subsequently different ZnO nanoparticles solutions were spin coated on top of the PEDOT:PSS layer. ZnO nanoparticles were synthesized according to reference [27], using the hydrothermal condensation of Zn(acetate). After several rinsing steps, the nanoparticles were re-dispersed in acetone or isopropanol. Resistance measurements indicate a conductivity drop by a factor 2, in for both ZnO dispersed in acetone and isopropanol (Fig. 11). Herein, the thickness of PEDOT:PSS layer remains unchanged. However, spin coating of the pure solvents on the PEDOT:PSS layer does not reveal conductivity changes of the PEDOT:PSS layer. This clearly confirms that the interaction between ZnO and PEDOT:PSS is responsible for the observed drop in conductivity in the PEDOT:PSS layer.

In several publications [28, 29] it has been shown that phase segregation occurs within the PEDOT:PSS layer, resulting in a predominance of PSS in the surface region. Thus deposition of ZnO on top of the PSS rich surface of PEDOT:PSS layer increases the chance of interaction between PSS and ZnO. Although PEDOT:PSS layer theoretically should be in a solid

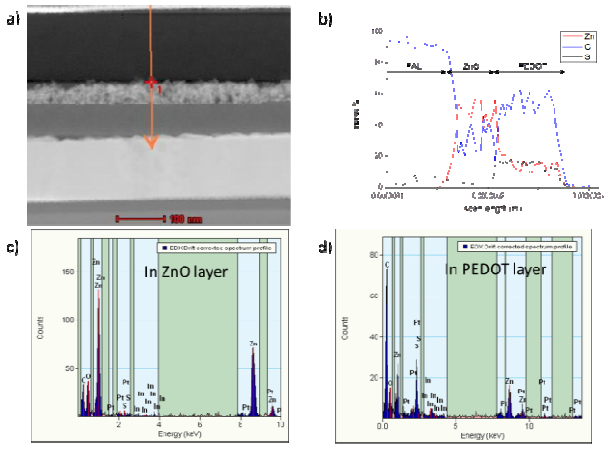

Fig. 12. EDX depth scan profile of the stack (from top) PAL/ZnO/PEDOT:PSS: (a) – SEM micrographs of FIB cross sections; (b) – mass percentage of the elements with scan length; (c) EDX drift corrected spectrum profile in ZnO layer and (d) EDX drift corrected spectrum profile in PEDOT:PSS layer.

Table 1. Device type and a necessity of high electric field treatments

Device type	Bottom electrode	ETL	PAL	HTL	Top electrode	High electric field required?
I	Ag/PEDOT	ZnO	P3HT:PCBM	PEDOT	Ag	Y
II	Ag/PEDOT	ZnO	P3HT:PCBM	MoO_3	Ag	N*
III	ITO/---------	ZnO	P3HT:PCBM	PEDOT	Ag	N
IV	ITO/PEDOT	ZnO	P3HT:PCBM	PEDOT	Ag	N*

* - these types of devices are working without necessity of high electric field treatments if compatible formulations of bottom PEDOT:PSS and ZnO are selected (as described above). However, if the same PEDOT:PSS and ZnO formulations are also applied for the device type IV, with two Ag contacts, such devices always require high electric field treatments.

state, moisture and solvents from the ZnO solution, which are nicely compatible with PEDOT:PSS, create favourable conditions for following reaction:

$$ZnO + 2H^+ \rightarrow Zn^{2+} + H_2O.$$

Zn^{2+} cations can easily migrate into the bulk of the PEDOT:PSS layer, which is proven by EDX depth scan profile of the OPV stack (Fig. 12). The presence of Zn (as an element) in the PEDOT:PSS layer is shown by EDX analyses, however, FIB SEM cross-sectional analyses does not show the presence of ZnO nanoparticles in that PEDOT:PSS layer, providing additional evidence that Zn in the PEDOT:PSS layer is most probably present in its cationic form and probably chelated by the PSS poly-anion.

As shown in Fig. 11, the conductivity of PEDOT:PSS layer after deposition of the ZnO layer drops by factor of 2, but still remains in the range of ~300 $S \cdot cm^{-1}$. With a thickness of 100 nm, it yields a sheet resistance of 300-350 Ohm/sq). It can slightly decrease the fill factor, but with an optimized grid geometry, this should not significantly reduce the performance of the devices. The most critical here is the decomposition of the ZnO layer, which is responsible for blocking the holes. This layer is typically very thin (~30 nm) and its decomposition can be very critical for its hole blocking and electron transport properties. Thus, increasing the thickness of ZnO layer is necessary not only for obtaining an uniform layer formation as described above, but also to compensate a thickness decrease due to interaction with the PEDOT:PSS, causing depletion of ZnO.

Photoactive layer

The next layer in the OPV stack is the photoactive layer. The performance of the devices depends largely on the quality of the photoactive layer. The uniformity of an inkjet printed photoactive layer is mostly determined by the ability of the individual droplets to merge, forming initially an uniform wet film prior to the drying process. Here are a lot of parameters responsible for the final quality of the layer, such as choice of solvent, printing and drying parameters. The optimal inkjet printing parameters, which did not affect the performance significantly with changing both the deposition method from spin-coating to inkjet printing and changing the solvents to a halogen-free solvent system, are reported previously [16].

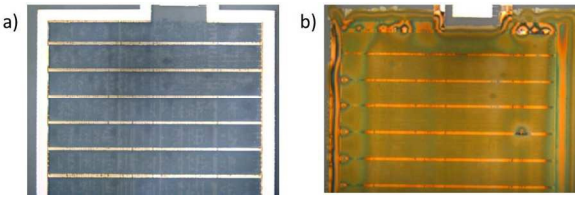

Fig. 13. Optical microscope image of OPV stack (inkjet printed Ag grid/PEDOT:PSS/ZnO/PAL) showing the non-uniformity in photoactive layer introduced by the non-uniformities in undelaying layers.

Apart from this, another important parameter which is responsible for the final quality of photoactive layer is the quality and uniformity of the layers underneath. Defects in underlying layers introduce defects in subsequent layer, as shown in Fig.13. As a result, such devices show leakage currents and/or shunts. Solving of this problem has a complex character as basically the defects in all layers underneath have to be avoided. Recommendations for avoiding defects in the Ag-grids, the PEDOT:PSS and ZnO layer are described above.

Top PEDOT:PSS

The presence of two PEDOT:PSS layers in one single device stack and its effect on the functioning of the device is still a subject to discussions. We found, and it was confirmed in other publications [17], that devices with two PEDOT:PSS layers require a short electric pulse to start functioning (device I in Table 1). Before the electric pulse, some of the as-made cells behave as an Ohmic resistor (right panel in Fig. 1c) that seems limited by the series resistance of the system, while others show a much higher shunt resistance (left panel in Fig. 1c). The fact that the extent of the shunting varies strongly, from almost absent to dominant, suggests that the shunt forming is incidental and not an intrinsic property of the layers. After the electric pulse, the *JV* curves are identical in Fig 1c. In some devices the shunt cannot be removed (Fig 1d), supporting the idea that the shunts are extrinsic. Interestingly, devices with an evaporated MoO_3/Ag back contact do not require high electric field post-treatments if defects in the all printed layers are eliminated (device II in Table 1). However, substitution of MoO_3 by PEDOT:PSS layer as hole transport material requires post treatments with high electric field.

Larsen-Olsen et al. [17] relate this behaviour to the redox nature of PEDOT:PSS [30] and propose that it can be switched by

a short electrical pulse. According to these authors an electrochemical reaction at the P3HT:PCBM - PEDOT:PSS interface occurs. Larsen-Olsen et al. [17] propose that as a result, PEDOT:PSS is de-doped and becomes an efficient hole selective contact. The short electric pulse would create a de-doped interface, which blocks electrons from the photoactive layer. Unfortunately, it proved difficult to obtain convincing experimental evidence for this mechanism. In our view, the statement that the P3HT:PCBM - PEDOT:PSS interface is responsible for the switching mechanism in the devices needs extra clarification. First of all, it has to be explained why this switching is not required for typical ITO-based devices with inverted architectures (device III in Table 1). It appears, that only devices with two PEDOT:PSS layers need applying an electric field to enable proper functioning (device I in Table 1). Second, in the proposed mechanism is necessary that holes are injected from the ZnO bottom contact side into the P3HT or electrons from the PEDOT top contact in to the PCBM, or both to explain the high currents under reverse bias before switching. That is unlikely because the energy barriers are high. If PEDOT is reduced the Fermi level in that layer will lie higher, enhancing (and not reducing) the possibility of electron injection. Hence if the reduction suggested by Larsen-Olsen et al occurs, the reverse current should be enhanced, not reduced. Third, the shunt burning happens in reverse bias when the field is such that the electron flow is opposite to the direction needed to reduce the PEDOT:PSS at the interface with the photoactive layer.

Similar resistive switching mechanisms have been utilized in write-once-read-many (WORM) memory devices [31, 32]. Möller et al. [31, 32] have observed permanent switching in PEDOT layers on top of a thin film silicon diode and attributed this phenomenon to a current-controlled, thermally activated un-doping of $PEDOT^+$ to $PEDOT^0$. Analogously, in a device configuration in which PEDOT is sandwiched between Al and ITO electrodes, Ha and Kim [30, 33] have observed bipolar switching. These devices could be switched on and off under forward and reverse bias. The switching behaviour of these devices was explained by the formation and destruction of a current path due to redox behaviour of PEDOT chains in the PEDOT:PSS film. A PEDOT:PSS thin film consists of p-doped PEDOT chains ($PEDOT^+$) and PSS. A highly conductive current path in formed by $PEDOT^+$ chains. The injection of holes into the PEDOT:PSS layer will create sufficient number of $PEDOT^+$ chains for a current path. The injection of electrons into PEDOT:PSS layer reduces $PEDOT^+$ to $PEDOT^0$ and destroys the current path. Therefore, the switching behaviour in WORM memory has permanent conductivity changes, from the "on" state to the "off" state. It is not evident that this mechanism is responsible for the shunting behaviour in the cells as, it would imply that the shunts could be switched on cells on and off again, which is not the case for the solar cells.

Marsman et al. [34] have reported the operating mechanism in WORM devices relies on the irreversible reduction of the electrical conductivity of polyaniline by Joule heating, similar to standard safety fuses. In this simple thermal model the fuse interrupts when the provided electrical power equals the thermal power. Finally, de Brito et. al. [35] have introduced the operating mechanism in the WORM devices driven by the delamination by gas formation upon electrolysis of water. They show that the critical voltage required for switching being constant and equal to the potential value for water electrolysis (typically around 2 V), indicating that electrolysis of water in the PEDOT/PSS is responsible for fuse interruption.

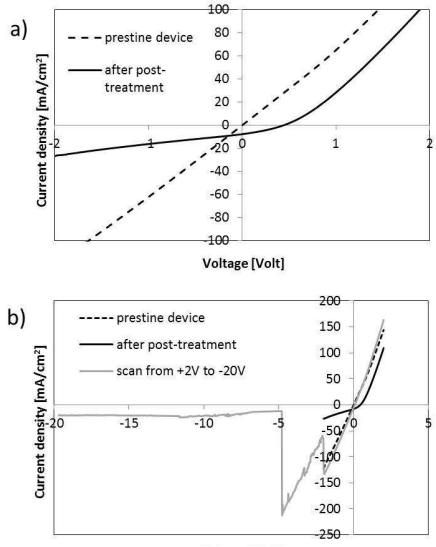

Fig. 14. (a) J-V curves of the pristine devices device and after post treatment at high electric field; (b) – scan of pristine devices from +2 to -20 V indicating an inflection point between non-working and working form of the device.

Given these largely different explanations it is not possible to provide an unambiguous mechanism for the switching at present. Experimental evidence for the reduction of $PEDOT^+$ to $PEDOT^0$, as put forward in several papers, is scarce. The reduced form was never identified spectroscopically. At present we favour an explanation in terms of a simple PEDOT-PEDOT short that that explains the high current in reverse bias before the shunt burning. The fact that the shunting is only observed for devices with two PEDOT layers may be somewhat coincidental and related to the roughness of the first PEDOT layer on the Ag grid. For a more smooth ITO bottom contact such shunts are less likely (Devices III and IV in Table I). For a top contact of MoO_3 (Device II in Table I) the lower lateral conductivity of MoO_3 and can explain the absence of shorts. Clearly further investigations are required to unravel the mechanism of the increased resistivity after an electric pulse in these solar cells, and prove or disprove explanations that have been suggested in the literature.

General approach

The presence of one failure mechanism in an OPV device does not exclude others. Most of the devices can be recovered with a short electric pulse. However, as there can be more than one failure mechanisms simultaneously occurring, often different voltages can be required to get devices working. Fig. 14 shows JVs of pristine devices and after post-treatment at

high electric field. However the post-treatment has been performed not as usual by applying high negative voltage for one second, but the devices was scanned from +2 V to -20 V, to visualize the transition point. The JV shows two jumps at -2 V and at -5 V, indicating that probably at least two different defects are removed at the corresponding applied voltages.

Conclusions

A detailed analysis of all possible failures in the devices has been performed. The results show that there are several mechanisms that could lead to device failure. The observed failures can be subdivided into three main groups:

- Failures due to unwanted short circuits, causing shunts. Such shunts can be formed by several artefacts, like *e.g.* a too high topology of the printed bottom Ag-grid or cracking of the grid lines, a bad quality of photoactive layer, a mis-alignment of the bottom and top electrode, particles, *etc*. Very often the shunts can be burned out by applying a high electric field. As the success of such a post-treatment depends on the amount and the size of the shunts, it is better to prevent artefacts from the beginning.

- Failures due to defects in the ZnO layer. The investigated device architecture contains symmetrical Ag/PEDOT:PSS contacts on both sides. Hence, the current flow in the devices largely depends on the electron harvesting properties of the ZnO. Defects and non-uniformities in ZnO layer can create efficient centres for charge recombination, providing high current leakage. Large holes or local absence of a ZnO layer will lead to a zone of a local symmetrical device. Such kind of failure cannot be recovered via some kind of a post-treatment process. The main recommendation in this case is assuring layer integrity by implementing good quality inks, deposition tools and processes and by proper monitoring the layer quality.

- Failures due to the presence of two PEDOT:PSS layers in the device, combined with weak electron blocking properties of PEDOT:PSS. Such type of failure requires a short electric pulse to activate or switch the devices to start working properly. It is assumed that a short electric pulse can make the interface of PEDOT:PSS selective for one type of charge.

The comprehensive analysis performed in this study allowed to identify the failure mechanism in the devices. Practical solutions to avoid identified failures are proposed. Proposed solutions were practically realised in manufacturing all-solution processed devices reported earlier [14, 16]. Understanding the failures mechanisms helped to produce functional devices with much higher manufacturing yield. Identifying and eliminating the defects at an early stage significantly reduced the time of process development and improved the reliability of the overall manufacturing process. The reported approach could also be exploited in OPV devices with other architecture and in other printed electronic devices. Understanding of possible failures can be very useful in problem prevention for further devices.

Acknowledgements

The work leading to this publication has received funding from the European Union Seventh Framework Programme (FP7/2007-2013) under grant agreement n° [281027] in the frame of Clean4Yield Project and from the European Community's Seventh Framework Programme (FP7-NMP-2013) in the frame of the MUJULIMA project (grant n#604148).

Notes and references

1. D. Angmo, T. T. Larsen-Olsen, M. Jørgensen, R. R. Søndergaard and F. C. Krebs, Adv. Energy Mater., 2013, **3**, 172-175.
2. Y. Lin, H. F. Dam, T. R. Andersen, E. Bundgaard, W. Fu, H. Chen, F. C. Krebs and X. Zhan, J. Mater. Chem. C, 2013, **1**, 8007-8010.
3. J. S. Yu, I. Kim, J. S. Kim, J. Jo, T. T. Larsen-Olsen, R. R. Søndergaard, M. Hösel, D. Angmo, M. Jørgensen and F. C. Krebs, Nanoscale, 2012, **4**, 6032-6040.
4. M. Helgesen, J. E. Carlé and F. C. Krebs, Adv. Energy Mater., 2013, **3**, 1664-1669.
5. T. R. Andersen, H. F. Dam, B. Andreasen, M. Hösel, M. V. Madsen, S. A. Gevorgyan, R. R. Søndergaard, M. Jørgensen and F. C. Krebs, Sol. Energy Mater. Sol. Cells, 2014, **120**, Part B, 735-743.
6. N. Espinosa, R. García-Valverde, A. Urbina, F. Lenzmann, M. Manceau, D. Angmo and F. C. Krebs, Sol. Energy Mater. Sol. Cells, 2012, **97**, 3-13.
7. N. Espinosa and F. C. Krebs, Sol. Energy Mater. Sol. Cells, 2014, **120**, 692-700.
8. N. Espinosa, F. O. Lenzmann, S. Ryley, D. Angmo, M. Hösel, R. R. Søndergaard, D. Huss, S. Dafinger, S. Gritsch, J. M. Kroon, M. Jørgensen and F. C. Krebs, J. Mater. Chem. A, 2013, **1**, 7037-7049.
9. Y. Galagan, E. W. C. Coenen, S. Sabik, H. H. Gorter, M. Barink, S. C. Veenstra, J. M. Kroon, R. Andriessen and P. W. M. Blom, Sol. Energy Mater. Sol. Cells, 2012, **104**, 32-38.
10. J. J. Van Franeker, W. P. Voorthuijzen, H. Gorter, K. H. Hendriks, R. A. J. Janssen, A. Hadipour, R. Andriessen and Y. Galagan, Sol. Energy Mater. Sol. Cells, 2013, **117**, 267-272.
11. D. Angmo, S. A. Gevorgyan, T. T. Larsen-Olsen, R. R. Søndergaard, M. Hösel, M. Jørgensen, R. Gupta, G. U. Kulkarni and F. C. Krebs, Org. Electron., 2013, **14**, 984-994.
12. J. E. Carlé, M. Helgesen, M. V. Madsen, E. Bundgaard and F. C. Krebs, J. Mater. Chem. C, 2014, **2**, 1290-1297.
13. P. He, C. Gu, Q. Cui and X. Guo, Proc. SPIE 8312, Display, Solid-State Lighting, Photovoltaics, and Optoelectronics in Energy III, 83120A (December 16, 2011); doi:10.1117/12.905678
14. T. M. Eggenhuisen, Y. Galagan, A. F. K. V. Biezemans, T. M. W. L. Slaats, W. P. Voorthuijzen, S. Kommeren, S. Shanmugam, J. P. Teunissen, A. Hadipour, W. J. H. Verhees, S. C. Veenstra, M. J. J. Coenen, J. Gilot, R. Andriessen and W. A. Groen, J. Mater. Chem. A, 2015, **3**, 7255-7262.
15. Y. Galagan, E. W. C. Coenen, R. Abbel, T. J. Van Lammeren, S. Sabik, M. Barink, E. R. Meinders, R. Andriessen and P. W. M. Blom, Org. Electron., 2013, **14**, 38-46.
16. T. M. Eggenhuisen, Y. Galagan, E. W. C. Coenen, W. P. Voorthuijzen, M. W. L. Slaats, S. A. Kommeren, S. Shanmuganam,

M. J. J. Coenen, R. Andriessen and W. A. Groen, Sol. Energy Mater. Sol. Cells, 2015, **134**, 364-372.
17. T. T. Larsen-Olsen, R. R. Sondergaard, K. Norrman, M. Jorgensen and F. C. Krebs, Energy Environ. Sci., 2012, **5**, 9467-9471.
18. D. Angmo, I. Gonzalez-Valls, S. Veenstra, W. Verhees, S. Sapkota, S. Schiefer, B. Zimmermann, Y. Galagan, J. Sweelssen, M. Lira-Cantu, R. Andriessen, J. M. Kroon and F. C. Krebs, J. Appl. Polym. Sci., 2013, **130**, 944-954.
19. N. Li, P. Kubis, K. Forberich, T. Ameri, F. C. Krebs and C. J. Brabec, Sol. Energy Mater. Sol. Cells, 2014, **120**, 701-708.
20. W. A. MacDonald, M. K. Looney, D. MacKerron, R. Eveson and K. Rakos, Plastics, Plast. Rubber Compos., 2008, **37**, 41-45.
21. E. M. Petrie, in Handbook of Adhesives and Sealants 2nd ed. edit. McGraw-Hill, New York, McGraw-Hill, New York, 2nd ed edn., 2006.
22. J. R. Greer and R. A. Street, Acta Mater., 2007, **55**, 6345-6349.
23. S. H. Ko, H. Pan, C. P. Grigoropoulos, C. K. Luscombe, J. M. J. Fréchet and D. Poulikakos, Nanotechnology, 2007, **18**, 345202.
24. J. Perelaer, B. J. De Gans and U. S. Schubert, Adv. Mater., 2006, **18**, 2101-2104.
25. K. Fukuda, T. Sekine, D. Kumaki and S. Tokito, ACS Appl. Mater. Interfaces, 2013, **5**, 3916-3920.
26. E. B. Gutoff and E. D. Cohen, Coating and Drying Defects: Troubleshooting Operating Problems, Wiley-Interscience.
27. W. J. E. Beek, M. M. Wienk, M. Kemerink, X. Yang and R. A. J. Janssen, J. Phys. Chem. B, 2005, **109**, 9505-9516.
28. S. A. Mauger, L. Chang, C. W. Rochester and A. J. Moulé, Org. Electron., 2012, **13**, 2747-2756.
29. G. Greczynski, T. Kugler, M. Keil, W. Osikowicz, M. Fahlman and W. R. Salaneck, J. Electron. Spectrosc. Relat. Phenom., 2001, **121**, 1-17.
30. H. Ha and O. Kim, Appl. Phys. Lett., 2008, **93**, 033309.
31. S. Möller, S. R. Forrest, C. Perlov, W. Jackson and C. Taussig, J. Appl. Phys., 2003, **94**, 7811-7819.
32. S. Möller, C. Perlov, W. Jackson, C. Taussig and S. R. Forrest, Science, 2003, **426**, 166-169.
33. H. Ha and O. Kim, Jpn. J. Appl. Phys., 2009, 48, 04C169
34. A. W. Marsman, C. M. Hart, G. H. Gelinck, T. C. T. Geuns, D. M. de Leeuw, J. Mater. Res., 2004, **19**, 2057-2060.
35. B. C. de Brito, E. C. P. Smits, P. A. van Hal, T. C. T. Geuns, B. de Boer, C. J. M. Lasance, H. L. Gomes, D. M. de Leeuw, Adv. Mater. 2008, **20**, 3750–3753.